THE JOURNAL OF PHYSICAL CHEMISTRY B

Article

pubs.acs.org/JPCB

Excited-State Electronic Properties of 6-Methylisoxanthopterin (6-MI): An Experimental and Theoretical Study

Goutham Kodali,[†,‡] Madhavan Narayanan,[†] and Robert J. Stanley*[,†]

[†]Department of Chemistry, Temple University, Philadelphia, Pennsylvania 19122, United States

[‡]Department of Biochemistry and Biophysics, University of Pennsylvania School of Medicine, 1004 Stellar-Chance Building, 422 Curie Boulevard, Philadelphia, Pennsylvania 19104-6059, United States

Supporting Information

ABSTRACT: 6-Methylisoxanthopterin (6-MI) is a pteridine-based guanine analog that has a red-shifted absorption and high fluorescence quantum yield. Its Watson−Crick base-pairing and base stacking properties are similar to guanine. The fluorescence quantum yield of 6-MI is sensitive to its nearest neighbors and base stacking, making it a very useful real-time probe of DNA structure. The fundamental photophysics underlying this fluorescence quenching by base stacking is not well understood. We have explored the excited-state electronic structure of the 6-MI in frozen 77 K LiCl glasses using Stark spectroscopy. These measurements yielded the direction and degree of charge redistribution for the $S_0 \rightarrow S_1$ transition as manifested in the difference dipole moment, $\Delta\vec{\mu}_{01}$, and difference static polarizability, $Tr\Delta\vec{\vec{\alpha}}$. TDDFT (time-dependent density functional theory) was employed to calculate the transition energy, oscillator strength, and the dipole moments of the ground and lowest optically bright excited state of 6-MI ($S_0 \rightarrow S_1$). The direction of $\Delta\vec{\mu}_{01}$ was assigned in the molecular frame based on the Stark data and calculations. These results suggest that the C4═O and C2-NH_2 groups are electron-deficient in the excited state, a very different outcome compared with guanine. This implies that Watson−Crick hydrogen bonding in 6-MI may be modulated by absorption of a photon so as to strengthen base pairing, if only transiently. Solvatochromism was also obtained for the absorption and emission spectra of 6-MI in various solvents and compared with the Stark spectroscopic results using both the Lippert-Mataga and Bakhshiev models.

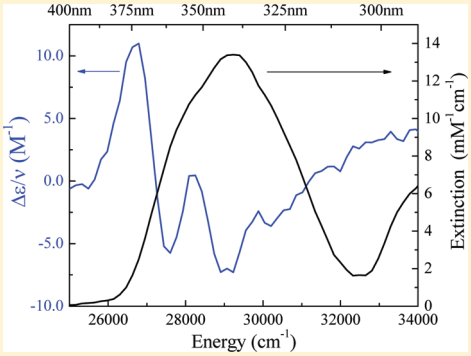

INTRODUCTION

6-Methylisoxanthopterin (6-MI), a pteridine-based guanine analog (Scheme 1), has been used to probe nucleic acid structure and dynamics. Its high fluorescence quantum yield (Φ_f = 0.70), combined with its red-shifted absorption (λ_{max} = 345 nm in water), provides for selective excitation in the presence of other native nucleic acids.[1,2]

Scheme 1. Chemical Structure of 6,8-Dimethylisoxanthopterin Used for the QM Calculations[a]

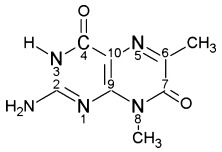

[a]The molecule used in the experiments was not the free base but 6-methylisoxanthopterinoside, where the sugar replaces the C8 methyl group.

6-MI is a fluorescent base pairing analog (FBA) of guanine: it forms Watson−Crick base pairs with cytosine. These base-pairing analogs (another example is 2-aminopurine (2AP), a fluorescent adenine analog[3−5]) tend to be dimmer than the larger pendant dyes often used to tag nucleic acids (e.g., fluorescein[6]). However, FBAs have more native base-like physical properties such as duplex melting point, steric footprints, and hydrogen bond patterns. Therefore, they are uniquely suited to act as fluorescent reporters of nucleic acid behavior.[7]

The emission quantum yield of 6-MI is sensitive to base stacking in DNA. We and others have examined this kind of behavior in other fluorescent adenine analogues like 2AP,[8−13] the pteridones 6MAP[14] and DMAP,[15] and 8-vinyladenine.[16,17] A common conjecture about the mechanism of fluorescence quenching in these FBAs is that excited-state electron transfer occurs with *FBA as the donor or acceptor depending on the redox potentials of its neighbors. We have shown this to be likely with 6-MI based on an electrochemical analysis, at least in the proximity of purines.[18] Steady-state fluorescence quenching experiments show that 6-MI is not quenched by pyrimidines.[19] This theme of purines quenching 6-MI more than by pyrimidines seems to be true whether in ssDNA or dsDNA.

Received: November 8, 2011
Revised: January 18, 2012
Published: January 25, 2012

dx.doi.org/10.1021/jp2110083 | J. Phys. Chem. B 2012, 116, 2981−2989

Electron transfer is not the only mechanism for emission quenching. It is now becoming apparent that other mechanisms may be at play. For example, Matsika et al. have shown that the accessibility of excited states to conical intersections leading to quenching may be unavailable to the monomer FBA because of large potential barriers.[20,21] These barriers can be lowered due to structural changes to the FBA that occur upon base stacking. These structural changes begin with charge redistribution of the molecule in the excited state after the absorption of a photon. Indeed, vectorial changes in excited-state charge density are responsible for initiating a number of important photobiological processes. These include the cis−trans photoisomerization of retinal,[22,23] hydrogen bond switching seen in BLUF domains (photoregulation of gene expression),[24] excited-state proton transfer in GFP,[25] and covalent photochemistry that results in biological signaling as found in the LOV domains.[26,27] In each case, charge redistribution is critical for altering the reactivity and properties of the photoexcited molecule relative to its ground state.

It should be emphasized that it is not just a change in the thermodynamic driving force of the reaction that is important (e.g., excited-state electron and proton transfer[28]) but that the excited-state charge density can lead to specific changes in bond orders. A simple example is found in the photoacidity of pyrenes,[29] where the details of the excited electronic structure modulates the pK_a^* of the molecule. Likewise, we have used Stark spectroscopy to obtain the excited-state electronic structure of 2-aminopurine and from this analysis suggested that certain hydrogen bonds might be significantly weakened due to a loss of electron density at the 2-amino nitrogen atom.[30] Therefore, the excited-state electronic structure of each FBA must be examined in detail as a monomer before its signature emission intensity in larger systems can be properly interpreted and exploited.

Here we have performed a low-temperature absorption and Stark spectroscopic analysis of the lowest optically allowed transition in 6-MI. These data afforded an estimate of the direction and magnitude of excited state charge redistribution. Solvatochromism studies were also performed to obtain complementary data based on changes in the spectrum of 6-MI as a function of solvent dielectric. TD-DFT calculations were used for ground- and excited-state charge densities, and the finite-field approach was applied to these calculations to generate simulated Stark spectra in a variety of continuum dielectrics to help assign the magnitude and direction of the difference dipole moment obtained from the Stark spectra. This calculated difference dipole moment is in good agreement with those obtained by both Stark spectroscopy and solvatochromism.

EXPERIMENTAL METHODS

6-MI nucleoside was a generous gift from Dr. Mary Hawkins (NIH) and was purified using a Rainin Dynamax HPLC equipped with a Dynamax (UV-1) UV/vis detector and HP 1046A fluorescence detector. A reverse-phase C-18 column (YMC ODS-AQ, 250 mm × 10 mm) was used with a 10−15% gradient of acetonitrile in water with 0.1% formic acid as the mobile phase at a flow rate of 1 mL/min to effect purification. Aqueous LiCl was used as a glass-forming matrix. Previous work on duplex DNA suggests that frozen LiCl glasses maintain DNA helical structure.[31−34] Because our long-term goal is to study FBA-containing duplex DNA using Stark spectroscopy, we initiated the monomer studies in this solvent.

Stark Spectroscopy: Experiment and Analysis. The basic setup of the Stark spectrometer has been previously described in detail.[30] Indium tin oxide (ITO)-coated quartz slides (100 Ω/cm^2) separated by two 55 μm kapton spacers formed the cuvette. Twenty-five μL of the 6-MI sample in 8 M LiCl was loaded into the cuvette mounted on a steel rod and immersed into liquid nitrogen. The angle of the sample with respect the polarization of light was varied by rotation of the rod with respect to the probe light. Light from a 150 W Xe arc lamp was filtered through 1/8-m monochromator with 2 nm band-pass. The monochromator was stepped in intervals of 88 cm^{-1}. After passing through the sample the probe light was focused with a quartz lens onto a silicon carbide photodiode (Sglux) and amplified by a current preamplifier. A 217 Hz sinusoidal applied electric field was generated from a Joe Rolfe HV amplifier fed by the sinusoidal output of the lock-in amplifier (SR 830, Stanford Research Systems). Typical field strengths were on the order of 4 × 10^5 V/cm. Phase-sensitive detection of the field-induced change in transmittance (ΔT) was obtained at 2ω using a 1 s time constant. Usually nine scans were taken and averaged together for a given Stark spectrum.

The low-temperature absorption spectrum was measured using the same setup by substituting an optical chopper for the AC power supply and detecting at ω. The transmittance of both the LiCl reference (I_0) and 6-MI/LiCl sample (I) were collected under the same conditions and absorbance spectra were calculated using Beer's law, $A = \log(I_0/I)$.

The analysis of Stark spectra derives from Liptay's approach[35] and details relevant to this study can be found in previous FBA Stark studies.[17,30] The relevant equation for the field-modulated spectrum is

$$\frac{\Delta\varepsilon}{\tilde{\nu}} = (f_c\vec{F})^2\left\{A_\chi\frac{\varepsilon(\tilde{\nu})}{\tilde{\nu}} + \frac{B_\chi}{15ch}\frac{d(\varepsilon(\tilde{\nu})/\tilde{\nu})}{d\tilde{\nu}} + \frac{C_\chi}{30c^2h^2}\frac{d^2(\varepsilon(\tilde{\nu})/\tilde{\nu})}{d\tilde{\nu}^2}\right\} \quad (1)$$

The term $\varepsilon(\tilde{\nu})$ represents the energy-weighted unperturbed extinction coefficient as a function of the energy $\tilde{\nu}$, $\vec{F}$ represents the electric field applied on the sample, and f_c is the local field correction factor for an elliptical solvent cavity.[36] An enhancement of the applied field is expected due to the cavity field of solvent matrix, which is dependent on the dielectric constant of the solvent. Because of this, f_c is always greater than one.[37] For LiCl, ε_0 = 15.[38] On the basis of the ground-state optimized structure (Figure S1 of the Supporting Information), the major axis a_x = 8.8 Å and the minor axis a_y = 6.2 Å, with a_z = 2.4 Å, corresponding to the width of two hydrogen atoms. The local field correction factor was estimated to be f_c = 1.63 based on an average of the a_x, a_y, and a_z.[36]

The derivative scaling factors A_χ, B_χ, and C_χ are related to intrinsic electronic properties of the chromophore and these properties are tied to the laboratory frame through χ, which is the angle between the direction of electric field vector of the linearly polarized light and that of the applied electric field $\vec{F}$. All of the Stark experiments reported here were performed with χ = 54.7° (magic angle) or 90°, after correcting for the refractive indices of liquid nitrogen and the ITO-coated quartz slides.

A_χ reflects the field-induced poling of a molecule possessing a ground-state dipole moment, but in a frozen glass $A_\chi \approx 0$.

dx.doi.org/10.1021/jp2110083 | J. Phys. Chem. B 2012, 116, 2981−2989

Information about the change in polarizability and the change in permanent dipole moment can be obtained from the coefficients B_χ and C_χ. The B_χ term is related to change in the polarizability, where

$$B_\chi \approx \frac{5}{2} Tr\Delta\vec{\vec{\alpha}} + (3\cos^2\chi - 1)\left(\frac{3}{2}\vec{m} \bullet \Delta\vec{\vec{\alpha}} \bullet \vec{m} - \frac{1}{2} Tr\Delta\vec{\vec{\alpha}}\right) \quad (2)$$

Here $\vec{m}$ is the transition dipole moment. The difference polarizability, $\Delta\vec{\vec{\alpha}} = \vec{\vec{\alpha}}_e - \vec{\vec{\alpha}}_g$, is a tensor, but for our purpose we consider only the trace of this polarizability, $Tr\Delta\vec{\vec{\alpha}}$, which is a scalar representing the polarizability volume. The trace of a tensor is invariant with respect to a change in coordinate system. Therefore, $Tr\Delta\vec{\vec{\alpha}}$ is a good estimate of the change in the polarizability volume upon excitation. The applied electric field will produce a second-derivative component of the absorption spectrum when the difference dipole moment, $\Delta\vec{\mu}$, is nonzero

$$C_\chi = |\Delta\vec{\mu}|^2\{5 + (3\cos^2\chi - 1)(3\cos^2\zeta_A - 1)\} \quad (3)$$

where ζ_A represents the angle between $\Delta\vec{\mu}$ and transition dipole moment $\vec{m}$, $\zeta_A^{0n} = \angle\vec{\mu}_{0n}\vec{m}_{0n}$ for the $S_0 \rightarrow S_n$ transition. When χ is the magic angle (54.7°), all χ-dependent values vanish and $\vec{\mu}$ can be obtained directly. A detailed description of the fitting procedure can be found in previous papers.[17,30] All determined values of $\Delta\vec{\mu}$ and $\mathrm{Tr}\Delta\vec{\vec{\alpha}}$ are reported in terms of debye and Å^3, respectively, where 1 debye (D) = 3.36×10^{-30} coulomb•meter and 1 Å^3 = 1.113×10^{-40} coulomb•meter^2/volt.

Solvatochromism: Experiment and Analysis. Methanol (MeOH), ethanol (EtOH), isopropanol (PrOH), butanol (BuOH), acetone (ACET), dimethylsulfoxide (DMSO), tetrahydrofuran (THF), chloroform (CHL), and water (H_2O) were spectroscopic grade and used as received. A 0.40 cm × 1.0 cm fluorescence quartz cell was used. The maximum optical density of the 6-MI solution was ~0.01.

Excitation and emission spectra of 2 μM solutions of 6-MI in each of these solvents were taken using a SPEX FluoroMax-2 fluorimeter (Horiba Jobin Yvon). The excitation spectra were collected with the emission wavelength set to 430 nm, and the emission spectra were collected with excitation at 345 nm unless otherwise noted. All spectra were collected with an integration time of 0.4 s/point, a 1 nm step size, and 2 nm excitation and emission slit widths. The spectra were solvent-corrected by subtracting excitation and emission spectra of the corresponding solvent. All spectra were corrected for any wavelength bias of the fluorimeter.

The Ooshika–Lippert–Mataga (OLM) equation defines the correlation between the solvent-dependent absorption and emission frequencies at their maximum intensities and the solvent properties as shown in eqs 4 and 5[39]

$$\tilde{\nu}_{abs} - \tilde{\nu}_{em} = \frac{2f_{OLM}(\varepsilon, n)}{hca^3}(\vec{\mu}_e - \vec{\mu}_g)^2 + C = \frac{2f_{OLM}(\varepsilon, n)}{hca^3}|\Delta\vec{\mu}|^2 + C = \Delta b_{OLM} f_{OLM}(\varepsilon, n) + C \quad (4)$$

where $\tilde{\nu}_{abs}$ and $\tilde{\nu}_{em}$ are the frequencies of the peak absorbance and fluorescence, respectively, h is Planck's constant, c is the velocity of light in vacuum, C is the energy difference at $f(\varepsilon,n) = 0$, and a is the radius of the solvated fluorophore including the first solvation sphere. In the OLM treatment, the dielectric properties of the solvent are found in the $f(\varepsilon,n)$ term

$$f_{OLM}(\varepsilon, n) = f(\varepsilon) - f(n) = \frac{\varepsilon - 1}{2\varepsilon + 1} - \frac{n^2 - 1}{2n^2 + 1} \quad (5)$$

where n is the solvent refractive index and ε is the dielectric constant. This treatment ignores the polarizability of the fluorophore and assumes that the ground and excited state dipole moments point in the same direction. A complete description of the terms in eqs 4 and 5 can be found in a previous reference.[17]

A more general treatment was formulated by Bilot and Kawski[40] based on Bakhshiev's analysis[41] (BKB model). They assumed that the polarizability of the fluorophore is the same as that of the solvent but that $\vec{\mu}_g$ and $\vec{\mu}_e$ are not necessarily parallel. Equation 4 then becomes[39,41−43]

$$\tilde{\nu}_{abs} - \tilde{\nu}_{em} = \Delta b_{BKB} f_{BKB}(\varepsilon, n) + C \quad (6)$$

where

$$f_{BKB}(\varepsilon, n) = \left[\frac{\varepsilon - 1}{\varepsilon + 2} - \frac{n^2 - 1}{n^2 + 2}\right]\frac{2n^2 + 1}{n^2 + 2} \quad (7)$$

and

$$\Delta b_{BKB} = \frac{2}{hca^3}(|\vec{\mu}_g|^2 + |\vec{\mu}_e|^2 - 2|\vec{\mu}_g||\vec{\mu}_e|\cos\theta) \quad (8)$$

where θ is the angle between $\vec{\mu}_g$ and $\vec{\mu}_e$. In either model, a plot of the Stokes shift $(\tilde{\nu}_e - \tilde{\nu}_g)$ versus the solvent polarization function $f(\varepsilon,n)$ will then yield the slope of the eq 4 or 6 and the excited-state dipole moment, $\vec{\mu}_e$, can be computed based on an estimate of $\vec{\mu}_g$ from computational methods.

Quantum Chemical Calculations. The ground-state geometry of 6,8-dimethylisoxanthopterin (6,8-DMI) was optimized using the TD-DFT package in Gaussian 03 at the B3LYP/6-311+G(d,p) level of theory. The solvent was modeled using the polarizable continuum model (PCM) developed by Mennucci et al.[44] The minimum energy structure was further confirmed by calculating vibrational frequencies at the same level of theory.

The excited-state energies, transition moments $\vec{m}_{0n}^C$, and ground- and excited-state permanent dipole moments $\vec{\mu}_n^C$ were calculated at the TD/B3LYP/6-311+G(d,p) level of theory. Permanent and transition dipole moment vectors using water as the PCM solvent were used in refining the assignment of the Stark parameters in the molecular frame. The $\vec{\mu}_n^C$ was used to calculate $\Delta\vec{\mu}_{0n}^C = \vec{\mu}_n^C - \vec{\mu}_0^C$. The PCM was used to include the effect of the dielectric response of the solvent (chloroform, methanol, ethanol, and water) on $\Delta\vec{\mu}_{0n}^C$. The difference electron density was calculated by subtracting the SCF ground-state density from the one-particle Rho-density for the corresponding excited states. Chemcraft (http://www.chemcraftprog.com) was used to generate and visualize the excited-state dipole moment vectors and difference density.

Difference dipole moments, $\Delta\vec{\mu}_{0n}^{FF}$, were calculated using the finite-field hexapole method where an external electric field propagating along the $\pm x$, $\pm y$, and $\pm z$ directions in the center of mass coordinates is applied in silico as previously described[17] and given by $E(\vec{F}) = E(0) - \sum_i \Delta\mu_i\vec{F}_i - {}^1/_2\sum_{ij}\Delta\alpha_{i,j}\vec{F}_i\vec{F}_j$. E is the vertical excitation energy and $\Delta\mu_i$ and $\Delta\alpha_{ij}$ are the vector and

dx.doi.org/10.1021/jp2110083 | J. Phys. Chem. B 2012, 116, 2981−2989

tensor components, respectively, of the change in the dipole moment upon optical excitation and the excess polarizability in the i and i, j directions.

Simulated Stark spectra were calculated by summing finite-field spectra computed for each axis ($\pm x$, $\pm y$, $\pm z$) and subtracting the zero-field spectra to generate field-on minus field-off spectra. The transition energies from the TD-DFT calculations were used to create a single Gaussian spectral line of 5 nm fwhm for each bright transition. However, vibronic structure has been omitted from the simulation so that the finite-field spectra represent only the overall effect of charge redistribution on the spectral shape.

RESULTS

Low-Temperature and Room-Temperature Absorption Spectra. The absorption spectra of 800 μM 6-MI at 77 and 298 K in 8 M LiCl are shown in Figure 1a. At room temperature, the maximum absorbance occurs at 29 400 cm^{-1} (340.1 nm) for the $S_0 \rightarrow S_1$ transition, and this transition begins to overlap with the $S_0 \rightarrow S_2$ transition at ~32 500 cm^{-1}. The spectrum is relatively featureless, but its numerical second derivative, shown in Figure 1b, shows possible vibronic structure. The absorption peak is identical, within experimental error, to that obtained by Seibert et al. for 6-MI in aqueous solution at pH 5.[45] This suggests that the effect of the high ionic strength of the frozen LiCl matrix on the ground and excited states of 6-MI is not significant.

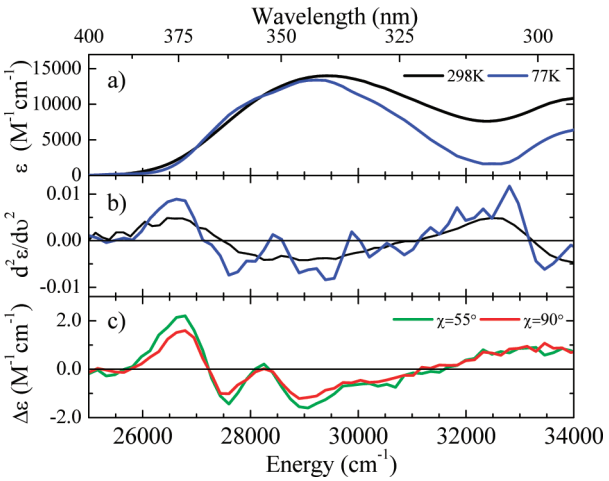

Figure 1. (a) Absorption spectra of 800 μM 6-MI in 8 M LiCl measured at room temperature (−) and at 77 K (blue −). (b) Second derivative of the room-temperature (−) and 77 K (blue −) absorption spectra. (c) Stark spectra for χ = 55 and 90° taken at 4.8 × 10^5 volts/cm.

The low-temperature spectrum is red-shifted by 160 cm^{-1}, peaking at 29 240 cm^{-1} (342.0 nm). There is a resolved shoulder at 27 600 cm^{-1} in the 77 K spectrum and a shoulder on the blue side of low energy band at 30 800 cm^{-1}. The second derivative spectrum (Figure 1b) shows a well-defined vibronic progression with a spacing of ~1626 cm^{-1} for the $S_0 \rightarrow S_1$ transition. The $S_0 \rightarrow S_2$ transition shows only one feature at 33 458 cm^{-1} due presumably to the limits of the spectral region scanned.

Stark Spectroscopy Results. The Stark spectra of 6-MI (800 μM) in 8 M LiCl solutions taken at 77 K at two different polarizations of light are shown in Figure 1c. They show a positive feature at 26 800 cm^{-1} and negative features at 27 600 and 29 060 cm^{-1}. The Stark spectrum is dominated by second derivative feature of the absorption spectrum, suggesting that there is a large difference dipole component contributing to charge redistribution. Interestingly, the small portion of the $S_0 \rightarrow S_2$ transition taken in these scans is relatively featureless. The Stark spectra show a polarization dependence, suggesting that the angle between transition dipole and difference dipole must be smaller than 54°.

The fitting of the Stark spectra was done assuming that there was no contribution below 32 000 cm^{-1} from the $S_0 \rightarrow S_2$ transition. A simultaneous fit of the absorption and Stark spectra was performed using zeroth, first, and second derivatives of the absorption spectrum. The fit (Figure 2a) shows a large second derivative contribution and nonzero first and zeroth derivative contributions. These components are shown in Figure 2b. The fitted C_χ term gives $|\vec{\mu}_{01}|$ = 5.1 ± 0.3D•f_c, and the fitted B_χ gives yields $Tr\Delta\vec{\vec{\alpha}}_{01}$ = 51 ± 10 Å$^3 f_c^2$ for the lowest energy optical transition. The angle between transition dipole and difference dipole is ζ_A = 28 ± 3°. These data, along with the solvatochromism results, are tabulated in Table 1.

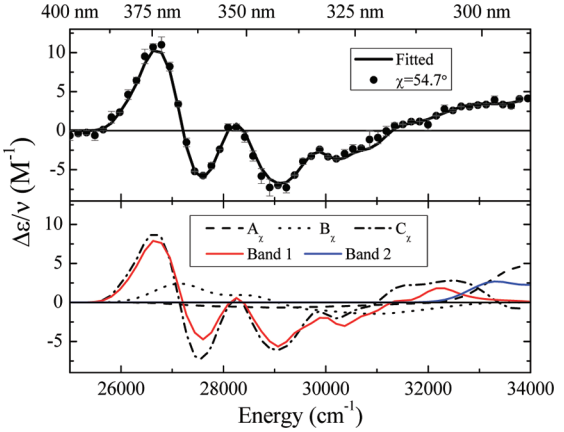

Figure 2. Top: Energy-weighted fit (−) to the 6-MI Stark spectrum for χ = 54.7°. Data are indicated by symbols with error bars from nine scans/spectrum with three spectra at each angle. Bottom: Summed derivative components of the fit (broken lines) along with the $S_0 \rightarrow S_1$ (red −) and $S_0 \rightarrow S_2$ (blue −) decomposition of the overall spectrum.

Even if the transition dipole moment $\vec{m}_{01}$ is known, there is still an infinite number of $\Delta\vec{\mu}_{01}$ that satisfy $\zeta_A \angle \Delta\vec{\mu}_{01},\vec{m}_{01}$. To assign $\Delta\vec{\mu}_{01}$ uniquely, TD-DFT was used to compute the ground-state permanent dipole and the transition dipole moments, $\Delta\vec{\mu}_0^C$ and $\vec{m}_{01}^C$. These vectors suggest that both ground-state and transition dipoles are in the plane of the molecule, leaving four possibilities for assigning $\Delta\vec{\mu}_{01}$ in the molecular frame. However, only one of these remaining vectors is in agreement with the $\Delta\vec{\mu}_{01}^{FF}$ calculated using the finite-field approach as well as $\Delta\vec{\mu}_1^C$ (Figure 3) and shown in Figure 4

Computational Results. The ground-state optimized geometry in water using the PCM is shown in Figure S1 of the Supporting Information (see below). The lowest energy transition $S_0 \rightarrow S_1$ in vacuum was 316 and 326 nm in water, compared with the experimental absorption spectrum peak at 340 nm, a 14 nm red shift relative to the computed spectrum. In order to assign the experimental $\Delta\vec{\mu}_{01}$ obtained from Stark spectroscopy, the direction of the transition dipole moment, $\vec{m}_{01}$, must be known. The magnitude and direction for $\vec{m}_{01}^C$

dx.doi.org/10.1021/jp2110083 | J. Phys. Chem. B 2012, 116, 2981−2989

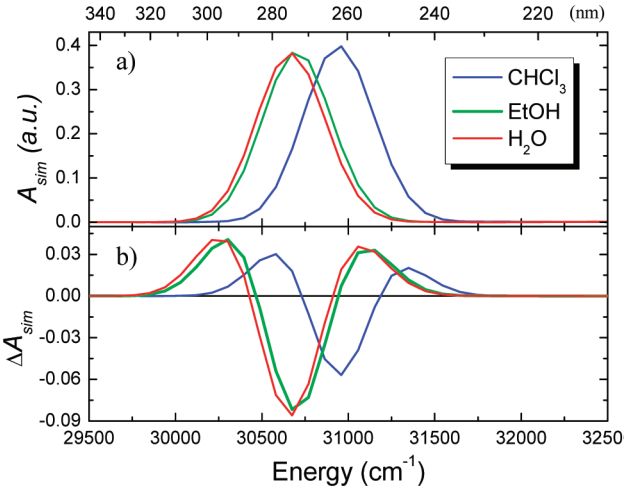

Figure 3. (a) Simulated absorption spectra (A_{sim}) in three solvents from the TD-DFT/finite-field approach. Only the E_{00} transition is shown for the $S_0 \rightarrow S_1$ band with a width of 5 nm. (b) Stark spectra (ΔA_{sim}) simulated from the finite-field difference approach.

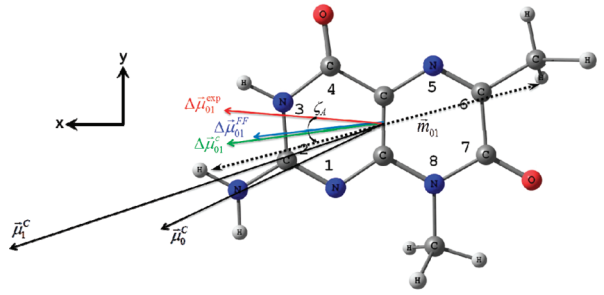

Figure 4. Permanent (solid black vectors), transition (dotted black vector), and difference dipole moments for the $S_0 \rightarrow S_1$ transition. All dipoles are computed with the exception of $\Delta\vec{\mu}_{01}^{exp}$ (solid red vector), which was obtained from the Stark measurement. Computed vectors are based on a PCM with water as the solvent. The axes are indicated with the positive z axis perpendicular to the plane of the page.

using the B3LYP/6-311+G(d,p) basis shows that $\vec{m}_{01}$ lies in the plane of the molecule, directed along C6−C2 axis, with components $m_X = -1.66$ D, $m_Y = 0.322$ D, and $m_Z = 0.0086$ D with an oscillator strength $f_{osc} = 0.274$. $\vec{m}_{01}^{C}$ makes an angle of 8° with the computed $\Delta\vec{\mu}_{01}$. Interestingly, Seibert et al. obtained $f_{osc} = 0.153$ for the $S_0 \rightarrow \pi\pi^*$ transition using MCSCF, in good agreement with our result, but the transition energy places the transition at 270 nm, clearly too low. They also used TD-DFT with a 6-31+G(d) basis set to obtain $f_{osc} = 0.032$ for the $S_0 \rightarrow \pi\pi^*$ transition (348 nm).

The ground-state and excited-state dipole moments directions did not change from vacuum to water, however their magnitudes increased by ~25%, consistent with prior observations.[17] Both the ground- and excited-state dipole moments were directed toward C6 (Table 2). The angle between the two vectors was 10.5°. The difference dipole moment, $\Delta\vec{\mu}_{01}^{C}$, is 4.79 D and points from the center of mass to the middle of the C2−N3 bond.

Table 1. Experimental Difference Moments for 6-MI

method	$\lvert\Delta\vec{\mu}_{01}\rvert$ (D)	$Tr(\Delta\vec{\alpha}_{01})$ (Å^3)	ζ_A (°)
Stark	3.2(0.2)[a]	16(3)	28(3)
BKB: HB	7.2	NA	NA
OLM: HB	11.6	NA	NA
BKB: All	5.4	NA	NA
OLM: All	9.7	NA	NA

[a] $f_c = 1.63$

Table 2. TD-DFT Computed Components of the Permanent Dipole Moments in Water (in Debye)

	$\vec{\mu}_X$	$\vec{\mu}_Y$	$\vec{\mu}_z$	$\vec{\mu}$
$\vec{\mu}_0$	10.61	−6.49	0.051	12.44
$\vec{\mu}_1$	15.39	−6.14	0.048	16.57
$\Delta\vec{\mu}_{01}$	4.78	0.35	−0.003	4.79

The difference density from these calculations is shown in Figure 5. A significant intramolecular charge separation occurs upon photoexcitation. There is net positive charge on the N1 nitrogen, the nitrogen of the amino group, and the oxygen of the C4 carbonyl group. Net negative charge appears on N5, C6, C7, and N8 atoms. This is consistent with the $\Delta\vec{\mu}_{01}$ direction given above.

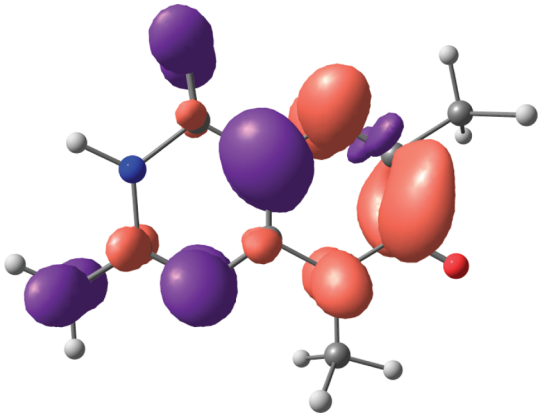

Figure 5. Electron difference density contours for the $S_0 \rightarrow S_1$ transition. Red corresponds to increased electron density, while blue represents electron-deficient parts of the molecule.

$\Delta\vec{\mu}_{01}$ was also calculated using wave functions derived from B3LYP and BHandHLYP functionals as input to the finite-field procedure (Table 3). The components of the $\Delta\vec{\mu}_{01}^{FF}$ dipoles are given in Table 3. $\lvert\vec{\mu}_{01}^{FF}\rvert$ values are 3.48 and 3.58 D for B3LYP and BHandHLYP, respectively. This is about 1 D lower compared with the $\Delta\vec{\mu}_{01}$ value calculated from ground-state and excited-state dipoles; however, the direction is same. Overestimation of the excited-state dipole using TD-DFT when charge transfer is significant has been well-documented.[46]

The computed $S_0 \rightarrow S_1$ Stark spectra of 6-MI in H_2O, EtOH, and $CHCl_3$ were obtained as described above and shown in Figure 3b. The absorption spectra are shown for comparison in Figure 3a. The spectra for H_2O (red line) and EtOH are very similar, with the lowest energy transition of 6-MI centered at ~326 nm dominated by a second-derivative feature. This suggests that the experimental spectra are consistent with a large difference dipole contribution.

Solvatochromism Results. 6-MI emission spectra were taken in various solvents to explore the effect of solvent polarity

dx.doi.org/10.1021/jp2110083 | J. Phys. Chem. B 2012, 116, 2981−2989

and hydrogen bonding ability on the emission yield and band shape. These data are shown in Figure 6. Fluorescence excitation spectra and emission spectra of 6-MI in the various solvents were peak-normalized (data not shown). The

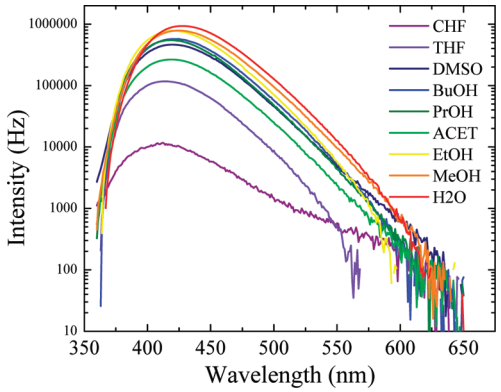

Figure 6. Emission spectra of 6-MI in various aprotic and protic solvents. The polarity of the solvent goes from lowest (purple) to highest (red).

corresponding Stokes shifts in the various solvents are listed in Table 4. The excitation maximum for 6-MI in water was

Table 3. Finite-Field Calculations (in Debye)

$\lvert\Delta\vec{\mu}_{01}\rvert(D)$	B3LYP/6-311+G(d,p)	BHandHLYP/6-311+G(d,p)
vacuum	2.02	0.99
chloroform	2.46	2.83
ethanol	3.34	3.50
water	3.48	3.58

found at 342 nm. A red shift in the excitation maximum was observed as a function of decreasing solvent polarity, although acetone showed a modest deviation from this expected trend.

6-MI fluorescence emission is the most red-shifted at 428 nm in water. The emission maxima blue shift with decreasing solvent polarity as expected. However, in *n*-butanol, the fluorescence emission red shifts to 425 nm. (See Table 4.) Again, this deviation is modest.

In the case of non-H-bonding solvents, no clear trend is observable as a function of changing solvent polarity. 6-MI in $CHCl_3$, DMSO, and THF exhibit the most blue-shifted excitation maxima at 346−350 nm, whereas the most red-shifted maxima were observed at 368 and 366 nm for DMF and ACN respectively (data not shown). Chloroform exhibits the most blue-shifted emission spectra with the λ_{max} at 412 nm, whereas that in DMF and ACN exhibited the largest red shifts with λ_{max} at 436 nm (data not shown). DMF and acetonitrile (as well as dioxane, studied here but not shown) are considered to be anomalous solvents with regard to their solvatochromism,[47] and we omit them from further consideration. However, a positive slope was obtained when plotting the solvent polarity function against the Stokes shifts using either the OLM or the BKB solvatochromism models, as shown in Figure 7.

The magnitudes of the difference dipole moment, $\lvert\Delta\vec{\mu}_{01}^{S}\rvert$, based on these solvatochromism models are shown in Table 1.

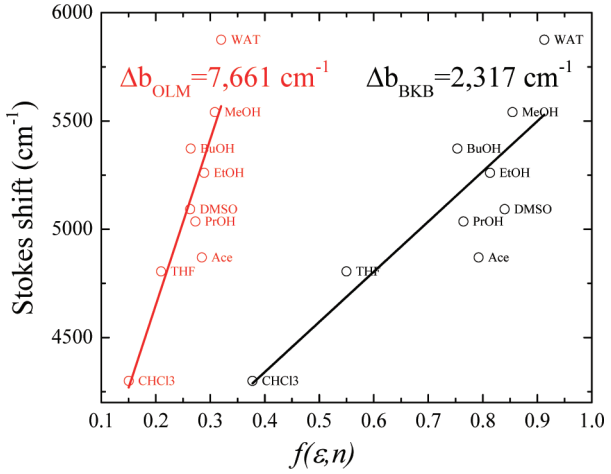

Figure 7. Analysis of solvatochromism of 6-MI using the OLM (red ○) and Bakhshiev (○) approaches. All indicated solvents were included in the linear fit, which is shown as a solid line. The slopes, Δb, for the models afford a determination of the excited state dipole moment.

The fit of the Stokes shifts against the solvent polarity function for 6-MI was done in two ways. In one case, only the H-bonding solvents were included. A second treatment included all solvents. $\lvert\Delta\vec{\mu}_{01}^{S}\rvert$ values from both the OLM and BKB analysis are strongly dependent on the radius of the solvated molecule. The computed radius of the solvated 6-MI nucleoside molecule is 5 Å (using DFT in Gaussian 03[48]). If we assume that $\vec{\mu}_g$ and $\vec{\mu}_e$ are in the same direction (OLM model), then $\lvert\Delta\vec{\mu}_{01}^{S}\rvert$ = 9.4 D. For the BKB model, $\lvert\Delta\vec{\mu}_{01}^{S}\rvert$ = 5.4 D is found for all solvents. However, it is not necessary for $\vec{\mu}_g$ and $\vec{\mu}_e$ to be in the same direction. The angle between $\vec{\mu}_g$ and $\vec{\mu}_e$ can be calculated directly from the magnitudes of $\vec{\mu}_g$ = 12.44 D and $\vec{\mu}_e$ =16.57 D (computed using TDDFT, see Table 2) using equation 8, which returns an angle of 13.7°. This is in very good agreement with the angle from the vectorial analysis of our theoretical results and the work by Seibert et al.[49] $\lvert\Delta\vec{\mu}_{01}^{S}\rvert$ for only the H-bonding solvents from the OLM and BKB models

Table 4. Solvent-Dependent Stokes Shift of 6-MI

solvent	$f_{OLM}(\varepsilon,n)$	$f_{BKB}(\varepsilon,n)$	λ_{EX} (nm)	$\tilde{\nu}_{EX}$ (cm^{-1})	λ_{EM} (nm)	$\tilde{\nu}_{EM}$ (cm^{-1})	$\Delta\tilde{\nu}$
chloroform	0.150	0.377	350	28571	412	24271	4299
THF	0.210	0.550	346	28901	415	24096	4805
DMSO	0.263	0.840	346	28901	420	23809	5092
BuOH	0.264	0.753	346	28901	425	23529	5372
PrOH	0.273	0.764	346	28901	419	23866	5035
acetone	0.285	0.792	348	28735	419	23866	4869
EtOH	0.289	0.813	344	29069	420	23809	5260
MeOH	0.309	0.854	344	29069	425	23529	5540
water	0.320	0.913	342	29239	428	23364	5875

dx.doi.org/10.1021/jp2110083 | J. Phys. Chem. B 2012, 116, 2981−2989

were 11.6 and 7.2 D, respectively. The $|\Delta\vec{\mu}_{01}^{S}|$ values from the analysis of all solvents and H-bonding solvents are overestimates compared with those measured by Stark spectroscopy and the computational results that we have reported in this work. The BKB model appears to be higher by a factor of 1.7 for all solvents and 2.3 for H-bonding solvents, whereas the OLM model is higher by a factor of 3.0 (all) and 3.6 (HB) compared with the $\Delta\vec{\mu}_{01}$ obtained using Stark spectroscopy. The large difference for the OLM approach can be attributed to the lower values of the dielectric function $(f(\varepsilon,n))$ in the OLM equation.

DISCUSSION

In this study, the lowest energy optically allowed transition of the fluorescent guanine analog 6-MI has been characterized by UV/vis absorption Stark spectroscopy and solvatochromism. The results were interpreted with the aid of TD-DFT calculations that returned permanent and transition dipole moments for the S_n states (n = 0,1). The magnitude and direction of the difference dipole $\Delta\vec{\mu}_{01}$ have been determined. In addition, finite-field calculations were performed to simulate the Stark spectra for $S_0 \rightarrow S_1$.

Beyond its initial characterization by Hawkins et al.,[1] a small number of groups have explored the excited-state properties of 6-MI monomer. Seibert et al. have measured the pH dependence of the fluorescence emission of the analog, showing that the N3 proton is labile.[45] These studies also gave absorption and emission maxima in aqueous solution at pH 5. Poulin et al.[19] explored the quenching of excited state 6-MI monomer by nucleobase monophosphates and found results roughly similar to our own Stern–Volmer study.[18]

Charge Redistribution in 6-MI Compared with Guanine Monophosphate. Luchowski and Krawczyk[50] have measured the Stark spectra of purine and pyrimidine native nucleic acid bases in ethylene glycol–water glasses at 100 K. For 6 mM 2° for GMP, they obtained $\Delta\vec{\mu}_{01}$ = 2.7(0.2) D•f_c which gives 1.7 D when f_c = 1.63, when compared to 3.2 D for 6-MI. This difference can be ascribed to the polarizing effect of the C7═O group of 6-MI. $\zeta_A = 26 \pm 2°$, is in good agreement with the value for 6-MI. The difference polarizability, $Tr\Delta\vec{\vec{\alpha}}_{01}$ = 15 ± 2 Å^3, is identical to that for 6-MI within experimental error. The difference in the transition dipoles of GMP and 6-MI, 7.1 and 12.4 D respectively, most likely is due to the above-mentioned polarizing effect.

One interesting difference is the relative directions of the transition dipole moment. In GMP, the dipole is along the short axis of the molecule, whereas in 6-MI it is closer to the long axis. In guanine, this charge redistribution would have little impact on hydrogen bonding between it and its Watson–Crick complement cytosine, partially due to the significantly lower $\Delta\vec{\mu}_{01}$ but, more importantly, due to the fact the direction of charge displacement is essentially orthogonal to the H-bonding triad. In 6-MI, as shown in Figure 5, the C4═O and C2-NH_2 groups of the triad show significantly lower electron density in the S_1 state. The C2-NH_2 group supplies 2 H-bond donor sites and the C4═O two H-bond acceptor sites (the lone pairs). A decrease in electron density at these sites will weaken the H-bond acceptor capacity at C4═O and strengthen the H-bond donor capacity at C2-NH_2. The unchanged HB-donor capacity at N3-H makes the excited state an overall better H-bond donor, suggesting that H-bonding in 6MI*:C is stronger than that in the ground state of 6MI:C or compared with the native G*:C. We have seen similar behavior in 2AP[30] and suggest that perhaps a transient change of hydrogen bonding may occur in these FBAs while the molecule is optically excited.

A further consequence of the large vectorial change in the excited-state electronic structure of 6-MI* is that the charge distribution in this state is the starting (Franck–Condon) point for the evolution of the excited-state potential. How the system evolves from this point will, in part, determine the electronic relaxation mechanism. Indeed, when incorporated into single-stranded or duplex DNA, this Franck–Condon initial excited-state charge distribution will see a very different potential energy landscape due to electronic and structural influences induced by neighboring bases, as suggested by Matsika and others.[20,51−54]

The large change in the difference dipole moment is a clear indication that the electron density of the excited state is quite different from the ground state. Because the molecule is probed at its ground-state equilibrium nuclear configuration, the dipole moment change will correlate with higher bond orders for some parts of the 6-MI framework and lower bond orders for other parts of the molecule. As mentioned in the Introduction, this change in excited-state bond energies can result in changes in excited-state pK_a, redox potentials, and hydrogen bond energies. The relative change, in both magnitude and direction, in the difference dipole moment is a valuable indicator of what mechanistic pathways can be justified on the basis of electronic structure. Indeed, we and others have used this same argument to rationalize the electron-transfer pathways in DNA photolyase.[55−57]

Comparison with Other QM Calculations. In an extensive computational study, Seibert, Ross, and Osman explored the structure of the electronic ground and excited states of 6-MI.[58] These calculations were performed using a variety of approaches, including second-order MP2 calculations to obtain an optimized ground-state geometry and TD-DFT (6-31G(d) and 6-31+G(d) bases) as well as CASSCF (6-31G(d) basis) calculations to characterize the excited states. Solvation was handled by the PCM.

Our B3LYP/6-311+G(d,p) TD-DFT optimized ground-state geometry is in excellent agreement with MP2-optimized ground-state geometry of Seibert et al. The largest structural deviation is the N1–C9 bond length, which is larger by +0.05 Å in the MP2 structure. The largest negative deviation is the −0.01 Å for the N3–H bond.

A comparison of the various dipole moments of 6-MI is not as straightforward. The transition dipole moments were calculated in water using the PCM. Using a 6-31G(d) basis for TD-DFT calculations with the B3LYP functional produced a low oscillator strength (f_{osc} = 0.03) at 343 nm, close to the observed wavelength. We obtained an oscillator strength of f_{osc} = 0.27 centered at 326.1 nm, well blue-shifted from the observed.

The experimental values of $\Delta\vec{\mu}_{01}$ = 3.2 ± 0.2 D with ζ_A = 28 ± 3° provide a basis of comparison with the quantum mechanical calculations. Seibert et al. found $\Delta\vec{\mu}_{01}$ = 2.86 D with ζ_A = 6.9° (using CASSCF) compared with our value of $\Delta\vec{\mu}_{01}^{C}$ = 4.79 D with ζ_A = 10.5° (using TD-DFT). The finite-field approach gave $\Delta\vec{\mu}_{01}^{FF} \approx$ 3.5 D (B3LYP and BandHLYP functionals), significantly lower than the TD-DFT approach but higher than the CASSCF calculation.

Beyond issues of specific basis sets and quantum mechanical procedures, all computational approaches applied to understanding

dx.doi.org/10.1021/jp2110083 | J. Phys. Chem. B 2012, 116, 2981–2989

the electronic structure of 6-MI fail to include specific solvent interactions such as hydrogen bonding. This is also the case in the solvatochromism results where the correlation of the solvent polarity with the Stokes shift is good but not robust. Therefore, in our view, the Stark experimental results give the most accurate picture of charge redistribution in the excited state. QM calculations support these results and provide a rational basis for assigning the direction of charge transfer in the molecular frame. Even here the experimentally determined ζ_A differs from the QM results by more than 15°.

CONCLUSIONS

The degree and direction of electronic charge redistribution in 6-MI in a low-temperature glass has been measured by absorption Stark spectroscopy. Charge redistribution in the lowest optically bright state is dominated by dipole moment changes. The difference dipole moment of the guanine analog is about twice that of GMP, whereas the difference polarizability and direction of charge displacement relative to the transition dipole moment are about the same. High-level TD-DFT and finite-field difference calculations were used to refine the experimental observations. The resulting picture of the excited state suggests that significant charge displacement occurs along the long axis of the molecule, with possible modulation of hydrogen bonding during excitation. Two solvatochromism models were also used to obtain the difference dipole moment of 6-MI and were compared with the Stark spectroscopy result.

ASSOCIATED CONTENT

Supporting Information

Optimized ground state geometry of 6-MI. This material is available free of charge via the Internet at http://pubs.acs.org.

AUTHOR INFORMATION

Corresponding Author

*E-mail: rstanley@temple.edu.

Notes

The authors declare no competing financial interest.

ACKNOWLEDGMENTS

We wish to thank Murali V.V.N.D and Dr. Rodrigo Andrade for help in providing dry-distilled solvents. We also wish to thank Dr. Vijay Singh for helpful discussions. G.K. and R.J.S. are grateful for support from the NSF Molecular Biosciences Division (MCB-0347087) and for a Temple University Bridge Grant. M.N. was supported by a grant from the NSF Division of Chemistry (CHE-0847855). This research was partially supported by grant number MCB080057P from the Pittsburgh Supercomputing Center, supported by several federal agencies, the Commonwealth of Pennsylvania, and private industry.

REFERENCES

(1) Hawkins, M. E.; Pfleiderer, W.; Balis, F. M.; Porter, D.; Knutson, J. R. *Anal. Biochem.* **1997**, *244*, 86−95.
(2) Hawkins, M. E. *Cell Biochem. Biophys.* **2001**, *34*, 257−281.
(3) Ward, D. C.; Reich, E.; Stryer, L. *J. Biol. Chem.* **1969**, *244*, 1228−1237.
(4) Evans, K.; Xu, D.; Kim, Y.; Nordlund, T. M. *J. Fluoresc.* **1992**, *2*, 209−216.
(5) Nordlund, T. M.; Xu, D.; Evans, K. O. *Biochemistry* **1993**, *32*, 12090−12095.
(6) Kool, E. T. *Acc. Chem. Res.* **2002**, *35*, 936−943.
(7) Wilson, J. N.; Kool, E. T. *Org. Biomol. Chem.* **2006**, *4*, 4265−4274.
(8) Yang, K.; Stanley, R. J. *Biochemistry* **2006**, *45*, 11239−11245.
(9) Christine, K. S.; MacFarlane, A. W. IV; Yang, K.; Stanley, R. J. *J. Biol. Chem.* **2002**, *277*, 38339−38344.
(10) Jean, J. M.; Hall, K. B. *Proc. Natl. Acad. Sci. U.S.A.* **2001**, *98*, 37−41.
(11) Jean, J. M.; Hall, K. B. *J. Phys. Chem. A* **2000**, *104*, 1930−1937.
(12) Jean, J. M.; Hall, K. B. *Biochemistry* **2002**, *41*, 13152−13161.
(13) Rachofsky, E. L.; Osman, R.; Ross, J. B. *Biochemistry* **2001**, *40*, 946−956.
(14) Yang, K.; Matsika, S.; Stanley, R. J. *J. Phys. Chem. B* **2007**, *111*, 10615−10625.
(15) Hawkins, M. E.; Pfleiderer, W.; Jungmann, O.; Balis, F. M. *Anal. Biochem.* **2001**, *298*, 231−240.
(16) Ben Gaied, N.; Glasser, N.; Ramalanjaona, N.; Beltz, H.; Wolff, P.; Marquet, R.; Burger, A.; Mély, Y. *Nucleic Acids Res.* **2005**, *33*, 1031−1039.
(17) Kodali, G.; Kistler, K. A.; Narayanan, M.; Matsika, S.; Stanley, R. J. *J. Phys. Chem. A* **2010**, *114*, 256−267.
(18) Narayanan, M.; Kodali, G.; Xing, Y.; Hawkins, M. E.; Stanley, R. J. *J. Phys. Chem. B* **2010**, *114*, 5953−5963.
(19) Poulin, K. W.; Smirnov, A. V.; Hawkins, M. E.; Balis, F. M.; Knutson, J. R. *Biochemistry* **2009**, *48*, 8861−8868.
(20) Liang, J. X.; Matsika, S. *J. Am. Chem. Soc.* **2011**, *133*, 6799−6808.
(21) Kozak, C. R.; Kistler, K. A.; Lu, Z.; Matsika, S. *J. Phys. Chem. B* **2010**, *114*, 1674−1683.
(22) Mathies, R.; Stryer, L. *Proc. Natl. Acad. Sci. U.S.A.* **1976**, *73*, 2169−2173.
(23) Locknar, S. A.; Peteanu, L. A. *J. Phys. Chem. B* **1998**, *102*, 4240−4246.
(24) Bonetti, C.; Mathes, T.; van Stokkum, I. H. M.; Mullen, K. M.; Groot, M.-L.; van Grondelle, R.; Hegemann, P.; Kennis, J. T. M. *Biophys. J.* **2008**, *95*, 4790−4802.
(25) Chattoraj, M.; King, B. A.; Bublitz, G. U.; Boxer, S. G. *Proc. Natl. Acad. Sci. U.S.A.* **1996**, *93*, 8362−8367.
(26) Briggs, W. R.; Tseng, T.-S.; Cho, H.-Y.; Swartz, T. E.; Sullivan, S.; Bogomolni, R. A.; Kaiserli, E.; Christie, J. M. *J. Integr. Plant Biol.* **2007**, *49*, 4−10.
(27) Kennis, J. T. M.; Crosson, S.; Gauden, M.; van Stokkum, I. H. M.; Moffat, K.; van Grondelle, R. *Biochemistry* **2003**, *42*, 3385−3392.
(28) Rehm, D.; Weller, A. *Isr. J. Chem.* **1970**, *8*, 259−271.
(29) Silverman, L. N.; Spry, D. B.; Boxer, S. G.; Fayer, M. D. *J. Phys. Chem. A* **2008**, *112*, 10244−10249.
(30) Kodali, G.; Kistler, K. A.; Matsika, S.; Stanley, R. J. *J. Phys. Chem. B* **2008**, *112*, 1789−1795.
(31) O'Neill, M. A.; Barton, J. K. *J. Am. Chem. Soc.* **2004**, *126*, 13234−13235.
(32) Barnes, J. P.; Bernhard, W. A. *J. Phys. Chem.* **1995**, *99*, 11248−11254.
(33) Eisinger, J.; Gueron, M.; Schulman, R. G.; Yamane, T. *Proc. Natl. Acad. Sci. U.S.A.* **1966**, *55*, 1015−1020.
(34) Neely, R. K.; Jones, A. C. *J. Am. Chem. Soc.* **2006**, *128*, 15952−15953.
(35) Liptay, W. Dipole Moments and Polarizabilities of Molecules in Excited Electronic States. In *Excited States*; Lim, E. C., Ed.; Academic Press: New York, 1974; Vol. *1*, pp 129−229.
(36) Premvardhan, L.; Peteanu, L. *Chem. Phys. Lett.* **1998**, *296*, 521−529.
(37) Bublitz, G. U.; Boxer, S. G. *Annu. Rev. Phys. Chem.* **1997**, *48*, 213−242.
(38) Wei, Y. Z.; Sridhar, S. *J. Chem. Phys.* **1990**, *92*, 923−928.
(39) Lakowicz, J. R. *Principles of Fluorescence Spectroscopy*, 3rd ed.; Springer: New York, 2006.
(40) Bilot, L.; Kawski, A. *Z. Naturforsch.* **1962**, *17a*, 621−627.
(41) Bakhshiev, N. G.; Knyazhanskii, M. I.; Minkin, V. I.; Osipov, O. A.; Saidov, G. V. *Usp. Khim.* **1969**, *38*, 1644−1673.

(42) Kawski, A. *Z. Naturforsch., A: Phys. Sci.* **2002**, *57*, 255−262.
(43) Jedrzejewska, B.; Kabatc, J.; Osmialowski, B.; Paczkowski, J. *Spectrochim. Acta, Part A* **2007**, *67A*, 306−315.
(44) Mennucci, B.; Tomasi, J. *J. Chem. Phys.* **1997**, *106*, 5151−5158.
(45) Seibert, E.; Chin, A. S.; Pfleiderer, W.; Hawkins, M. E.; Laws, W. R.; Osman, R.; Ross, J. B. A. *J. Phys. Chem. A* **2003**, *107*, 178−185.
(46) Dreuw, A.; Head-Gordon, M. *Chem. Rev. (Washington, DC, U.S.)* **2005**, *105*, 4009−4037.
(47) Reichardt, C. *Solvents and Solvent Effects in Organic Chemistry*; VCH Verlagsgesellschaft: Weinheim, Germany, 1988.
(48) Frisch, M. J.; Trucks, G. W.; Schlegel, H. B.; Scuseria, G. E.; Robb, M. A.; Cheeseman, J. R.; J. A. Montgomery, J.; T. Vreven, K. N. K.; J. C. Burant, J. M. M.; Iyengar, S. S.et al. *Gaussian 03*, revision A.1; Gaussian, Inc.: Pittsburgh, PA, 2003.
(49) Seibert, E.; Ross, J. B. A.; Osman, R. *Int. J. Quantum Chem.* **2002**, *88*, 28−33.
(50) Luchowski, R.; Krawczyk, S. *Chem. Phys.* **2005**, *314*, 309−316.
(51) Santoro, F.; Barone, V.; Improta, R. *J. Am. Chem. Soc.* **2009**, *131*, 15232−15245.
(52) Burghardt, I.; Cederbaum, L. S.; Hynes, J. T. *Comput. Phys. Commun.* **2005**, *169*, 95−98.
(53) Jean, J. M.; Hall, K. B. *Biochemistry* **2004**, *43*, 10277−10284.
(54) Worth, G. A.; Cederbaum, L. S. *Chem. Phys. Lett.* **2001**, *338*, 219−223.
(55) Kodali, G.; Siddiqui, S. U.; Stanley, R. J. *J. Am. Chem. Soc.* **2009**, *131*, 4795−4807.
(56) Medvedev, D.; Stuchebrukhov, A. A. *J. Theor. Biol.* **2001**, *210*, 237−248.
(57) Prytkova, T. R.; Beratan, D. N.; Skourtis, S. S. *Proc. Natl. Acad. Sci. U.S.A.* **2007**, *104*, 802−807.
(58) Seibert, E.; Ross, J. B. A.; Osman, R. *Int. J. Quantum Chem.* **2002**, *88*, 28−33.